ACS APPLIED MATERIALS & INTERFACES

Research Article

www.acsami.org

Magnetoresistance Effect in Rubrene-Based Spin Valves at Room Temperature

Xianmin Zhang,*[,†,‡] Qinli Ma,[‡] Kazuya Suzuki,[‡] Atsushi Sugihara,[‡] Gaowu Qin,*[,†] Terunobu Miyazaki,[‡] and Shigemi Mizukami[‡]

[†]Key Laboratory for Anisotropy and Texture of Materials (Ministry of Education), Northeastern University, Shenyang 110819, China

[‡]World Premier International Research Center, Advanced Institute for Materials Research, Tohoku University, Sendai 980-8577, Japan

Supporting Information

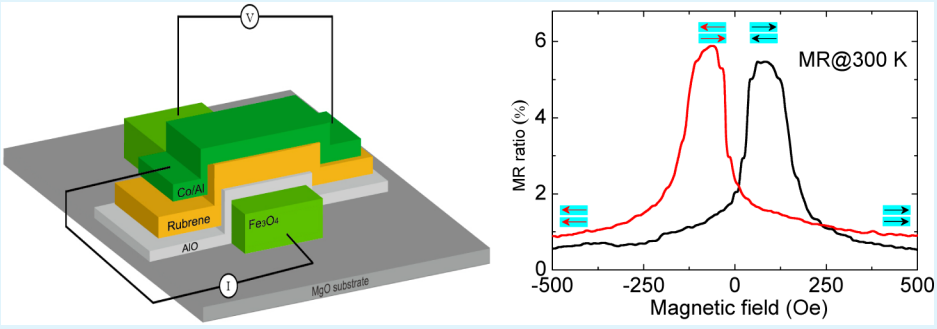

ABSTRACT: We fabricate spin-valve devices with an Fe_3O_4/AlO/rubrene/Co stacking structure. Their magnetoresistance (MR) effects at room temperature and low temperatures are systemically investigated based on the measurement of MR curves, current−voltage response, etc. A large MR ratio of approximately 6% is achieved at room temperature, which is one of the highest MR ratios reported to date in organic spin valves. With decreasing measurement temperatures, we observe that the MR ratios increase because of decrease in spin scattering, and the width of the MR curves becomes larger owing to increase in the coercivity of the electrodes at low temperature. A nonlinear current−voltage dependence is clearly observed in these organic spin valves. From the measurement of MR curve for the spin valves with different rubrene layer thickness, we observe that the MR ratios monotonously decrease with increasing rubrene-layer thickness. We discuss the spin-dependent transport mechanisms in these devices based on our experimental results and the present theoretical analysis. Moreover, we note that the devices exhibit smaller MR ratios after annealing compared to their counterparts without annealing. On the basis of atomic force microscopy analysis of the organic films and device resistances, we deduce that the increase of interface spin scattering induced by large surface roughness after annealing most probably leads to reduction in the MR ratios.

KEYWORDS: *rubrene, organic spintronics, spin valves, magnetoresistance effect, interface spin scattering*

INTRODUCTION

Organic spintronics devices have attracted extensive research interest because they combine the advantages of spintronics and organic semiconductors.[1−14] These devices can be used to manipulate the properties of spin and charge inherent in electrons, and the organic nature of such microelectronic devices could provide high structural flexibility, low production cost, and large area processing. Importantly, the strength of the spin−orbit interaction in organic semiconductors is considerably weaker when compared with that in inorganic materials as most organic semiconductors comprise elements with low atomic numbers.[1,2,14] This makes the spin relaxation time in an organic semiconductors longer than that in an inorganic counterparts. Hereby, organic device is ideal to fully modulate and utilize the spin of the electron to construct novel organic functional devices for next-generation applications. Organic spin valves (OSVs) is one of the most popular devices in organic spintronics. Typically, OSVs can be classified as lateral structure devices[1] and vertical structure devices[2] based on the device structure. Both types of structures are composed of two ferromagnetic (FM) electrodes separated by an organic semiconductors spacer layer. The magnetoresistance (MR) effect in the spin valve device is the phenomenon of change in the electrical resistance depending on the magnetization alignment of the two FM electrodes that are modified by an external magnetic field. A larger (smaller) resistance is usually observed when the magnetization directions are antiparallel (parallel). This phenomenon can be utilized to investigate spin transport properties in OSV devices.

Received: November 21, 2014
Accepted: February 10, 2015
Published: February 10, 2015

DOI: 10.1021/am508173j
ACS Appl. Mater. Interfaces 2015, 7, 4685−4692

Dediu et al. reported the fabrication of the first lateral spin valve using a 6T molecule as the spacer and $La_{0.67}Sr_{0.33}MnO_3$ (LSMO) as the electrodes.[1] Xiong et al. fabricated a vertical OSV device with 8-hydroxyquinoline aluminum (Alq_3) as the spacer layer between LSMO and Co electrodes, and they observed a negative MR ratio of 40% at 11 K.[2] Subsequently, large numbers of studies about OSVs have been performed by utilizing the FM electrode with high spin polarization and high Curie temperature, or introducing an insert layer to improve interface properties for efficient spin transport. Among of these investigations, achieving a high MR ratio at room temperature is a primary objective for potential applications.[13−16] One of the important issues to address in realizing high MR ratio in OSVs is the conductivity mismatch between the organic layer and the FM electrode, which increases the electron scattering at the interface and significantly reduces electron injection/detection at the organic/electrode interfaces. FM electrodes, such as Fe and Co, exhibit excellent conductivity. In contrast, organic semiconductors usually exhibit low carrier mobility. Therefore, organic semiconductors with high carrier mobility can be expected to achieve high MR ratios in OSVs.

Rubrene (5,6,11,12-tetraphenylnaphthacene) has a high carrier mobility[17] that is larger by 1 order of magnitude than that of 6T and by 5 orders of magnitude than that of Alq_3.[14,18] Moreover, the admixture parameter for spin−orbit coupling in rubrene is approximately 1 order of magnitude smaller than those of 6T and Alq_3 and a relatively large spin diffusion length has been predicted in rubrene.[19] Rubrene spin valves have been previously investigated in several studies. Yoo and co-workers fabricated a device with an LSMO/LAO/rubrene/V(TCNE) stacking structure, and they obtained an MR ratio of 4.7% at 100 K for a device with a 5 nm-thick rubrene layer.[20] By replacing the V(TCNE) electrode with an Fe electrode, the authors obtained a high MR ratio of over 12% at 10 K[21] and studied the effects of bias voltage and measurement temperature on giant MR response.[22] Moreover, Li et al. reported the fabrication of an Fe/rubrene/V(TCNE) spin valve with an MR ratio of 0.1% at 100 K using a 10 nm-thick rubrene layer.[23] Li et al. were also the first to successfully fabricate an all-organic based spin valve with a V(TCNE)/rubrene/V(TCNE) structure. The MR ratio of the device was 0.05% at 120 K with a 10 nm-thick rubrene layer.[24] In a spin valve with a EuS/rubrene/Fe structure, Raman et al. observed that the MR ratios increased with increasing bias voltage, and a high MR ratio of 6% was observed at 1 K.[25] In rubrene nanowire spin valves, Alam et al. reported the significant suppression of spin relaxation.[26] While the above works show obvious progress for understanding the spin transport behaviors in rubrene-based spin valves, achieving an MR response at room temperature are relatively rare.[27,28] Shim et al. directly measured a large spin diffusion length of 13.3 nm at 0.45 K in amorphous rubrene layer by spin polarized tunneling and obtained an MR ratio of 6% at 300 K in a Co/Al−O/rubrene/Fe stacking structure.[27] Lin et al. proposed an experimental method to analyze tunnelling and injection for spin transport mechanism and got an MR ratio around 3.5% at 300 K in a Co/AlO_x/rubrene/Fe stacking structure.[28]

In this Research Article, we report on a novel OSV device with an MgO-substrate/Fe_3O_4/Al−O/rubrene/Co/Al stacking structure. The utilization of Fe_3O_4 as electrode because of its high Curie temperature and high spin polarization,[29,30] which could enhance the spin transport efficiency at room temperature.[15,31,32] The MR response of the device were systemically investigated, and an MR ratio of ∼6% was obtained at room temperature, which value is one of the highest MR ratios reported to date in organic spintronics.[2,7,9,11−16,20−28,33−40] We studied the MR ratio dependence on the rubrene layer thickness and examined the spin-dependent transport mechanisms by characterizing the devices at different temperatures. In addition, we also explored the effect of annealing on the MR response in rubrene spin valves and discussed the strategy to further enhance device performance. The results of our study can provide deep understanding of the spin-dependent electron transport in organic spin devices.

EXPERIMENTAL SECTION

The Fe_3O_4 (100 nm) electrode was grown on a MgO (001) single-crystal substrate via RF magnetron sputtering with a shadow mask aligned to form a strip. The substrate temperature was maintained at 673 K during Fe_3O_4 deposition. An Al (2 nm) film was then deposited by RF magnetron sputtering on top of the Fe_3O_4 layer, which subsequently formed an Al−O layer via plasma oxidation. The above film sample was annealed in situ for 1 h at 623 K. After the samples were cooled to room temperature, they were taken out of the vacuum chamber. The rubrene layer was grown by thermal evaporation with a circular shadow mask in a different chamber. The film thicknesses were measured with a quartz crystal resonator. Without breaking the vacuum, the sample was transferred to a connected chamber to deposit a Co layer (10 nm) by DC sputtering. A new shadow mask was inserted to form a Co strip to pattern a cross configuration. Finally, Al (5 nm) was deposited to prevent Co oxidation. The circular shadow mask was left in place to protect the surface of the rubrene layer when the Co and Al mask was inserted. A small electric power of 10 W for up Co and Al deposition were used to reduce the kinetic energy of sputtered atoms. The area of device was 1.5 × 1.5 mm^2. The magnetization curves were measured using a vibrating-sample magnetometer with an applied field parallel to the film plane. The MR curves were measured via the standard four-probe method using a physical property measurement system (Quantum Design). The current−voltage curves were measured using a nanovoltmeter (model 2182A, KEITHLEY Inst. Inc.) and an AC and DC current source (model 6221, KEITHLEY Inst. Inc.). X-ray diffraction (XRD: Smartlab, Rigaku Co.) measurement using Cu K_a radiation was performed to characterize the structures of rubrene films. Atomic force microscopy (SII Seiko Instruments, SPA 400) was used to measure the surface images of the organic films.

RESULTS AND DISCUSSION

Figure 1a shows a schematic diagram of rubrene-based spin valve device structure. The rigid energy band diagram is drawn in Figure 1b. It is found that the energy levels of Fe_3O_4, rubrene and Co are well matched. Thereby, spin-dependent transport could be realized in our OSVs. Figure 2a is the magnetization curves for individual electrodes of MgO-substrate/Fe_3O_4/Al−O (red curve) and Si/SiO_2/rubrene/Co (black curve), which were measured at 300 K. It is observed that the coercivities for Fe_3O_4 and Co were near 145 and 15 Oe, respectively. The different coercivities could induce magnetization alignments with antiparallel and parallel alignments in the spin-valve devices. The saturation magnetization intensities were 380 emu/cc and 1450 emu/cc for Fe_3O_4 and Co, respectively. The value of intensities was closer to their bulk counterparts, indicating good film qualities. MR effect was evaluated by applying magnetic field along the direction of Fe_3O_4 strip. The MR curves for the rubrene-based spin valves were measured at different temperatures (300, 250, 200, and 150 K). Figures 2b and 2c show the MR curves for the devices with 2 nm-and 6 nm-thick rubrene layers, respectively. We observed that the MR steps appeared at

DOI: 10.1021/am508173j
ACS Appl. Mater. Interfaces 2015, 7, 4685−4692

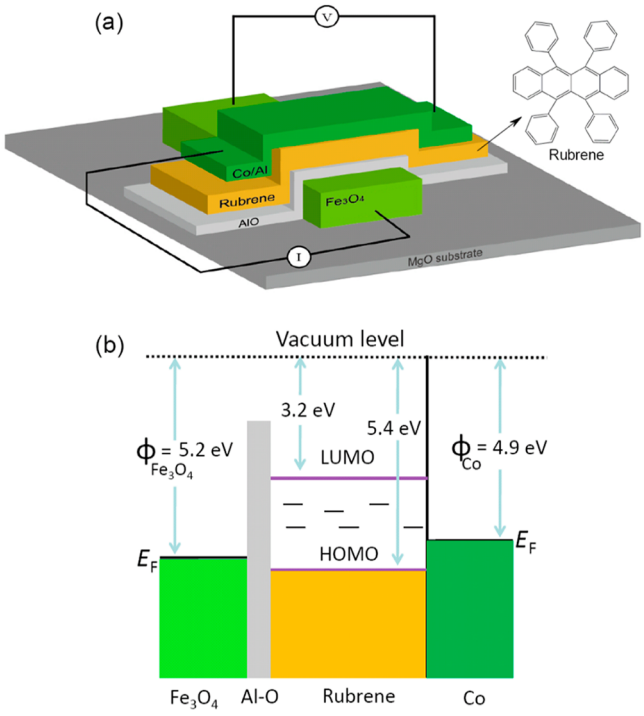

Figure 1. (a) Schematic diagram of rubrene spin valve device structure. The right inset shows a planar structure of rubrene molecule. (b) The rigid energy band diagram for the device showing the Fermi levels (E_F) and the work functions of Fe_3O_4 and Co, respectively, and the highest occupied molecular orbital (HOMO) and the lowest unoccupied molecular orbital (LUMO) levels of rubrene. The short lines between HOMO and LOMO levels depict possible defect states within rubrene layer.

around ±110 Oe owing to the antiparallel magnetization alignments of the Fe_3O_4 and Co electrodes, which is consistent with the result in Figure 2a. We calculated the MR ratio according to the following equation: $\Delta R/R_p = (R_{ap}/R_p - 1) \times 100\%$, where R_{ap} and R_p denote the resistances for the antiparallel and parallel states in the magnetization direction, respectively. The value for R_p was obtained with a magnetic field of 3000 Oe. The MR ratio was approximately 6% for the devices with a rubrene-layer thickness of 2 nm, as shown in Figure 2b. This is one of the highest MR ratios at room temperature in rubrene-based spin valves reported to date.[20−28] Upon reducing the measurement temperature, we observed that the width of the MR curves increased mainly because of increase in the coercivity of the Fe_3O_4 electrode. Meanwhile, the MR ratios were also enhanced with decreasing measurement temperatures. The MR ratios reached values of up to 7.2%, 8%, and 11% for temperatures of 250, 200, and 150 K, respectively. The increase in the MR ratio basically originates from the decrease of spin scattering at lower temperatures.[33] The temperature dependences of the MR ratios and MR curves for device with the 6 nm-thick rubrene layer were similar to those for the device with the 2 nm-thick rubrene layer. However, the MR ratio of the device with the 6 nm rubrene layer was smaller than that of 2 nm rubrene-layer device. The former exhibits MR ratios of 3.3%, 4.1%, 7%, and 9% corresponding to the temperature at 300, 250, 200, and 150 K, respectively. Without rubrene layer, MR effect does not appear in the spin valve of Fe_3O_4/Al−O/Co/Al with the same size as rubrene-based spin valve device. This can be understood by considering the low conductivity of Fe_3O_4 compared to

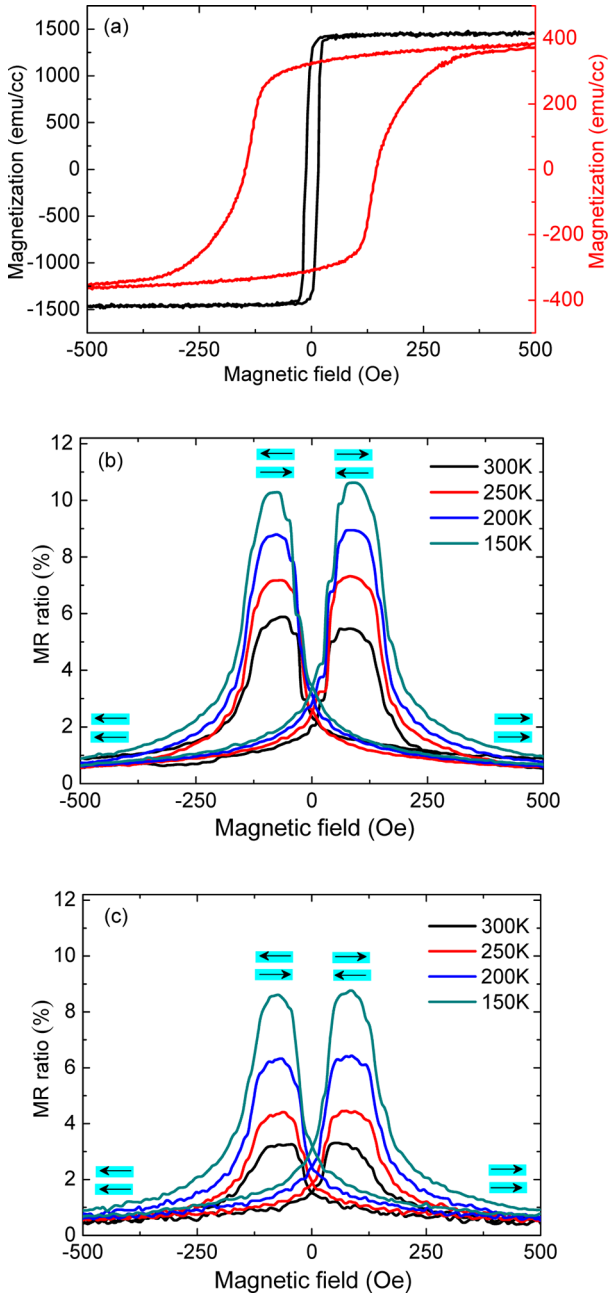

Figure 2. Magnetization curves for individual electrodes of MgO/Fe_3O_4/Al−O (red curve) and Si/SiO_2/rubrene/Co (black curve), which were measured at 300 K (a). Magnetoresistance curves for organic spin valve devices composed of (b) 2 and (c) 6 nm thick rubrene layers. The devices were measured at 300, 250, 200, and 150 K, respectively. The arrows illustrate the magnetization alignments in the antiparallel and parallel directions. The bias voltage for the measurement was fixed at 5 mV.

metal. According to our previous investigation[41] and the literature,[42] the device resistance for metal/Al−O/metal with the size of 1.5 × 1.5 mm^2 should be below 20 Ω. The voltage is shared most by the Fe_3O_4 electrode in Fe_3O_4/Al−O/Co/Al junctions, rather than the device. Thus, MR effect cannot appear in the inorganic junction, and only one negative and weak anisotropic MR effect from Fe_3O_4 electrode was observed.[12] By a combination of ultraviolet optical lithography and Ar-ion dry etching techniques, we fabricated the Fe_3O_4/Al−O/Co/Al junctions with sizes ranging from 10 × 10 to 30

DOI: 10.1021/am508173j
ACS Appl. Mater. Interfaces 2015, 7, 4685−4692

× 30 μm^2. This fabrication process cannot be used to prepare OSVs because it easily destroys molecular layer. The inorganic junctions show the MR ratios around 12%−15%. This is the maximum for the MR response in our present Fe_3O_4 electrode spin valves. Introducing buffer layers or further optimizing the fabrication could enhance MR ratios for inorganic Al−O junctions.[42]

The current−voltage curves for the devices with rubrene layer (6 and 20 nm) were measured at 300 and 150 K. Nonlinear current−voltage dependences were observed, as shown in Figure 3a and 3b. A similar nonlinear dependence for the device with 2 nm-thick rubrene layer was plotted in Supporting Information Figure S1. Moreover, with increasing rubrene-layer thickness, the nonlinear response of current−voltage dependences became stronger because of increase in the device resistance. Figure 3c depicts the clear bias-voltage dependence of MR ratios measured at 300 K (black circles) and 150 K (red squares) for a device with a 6 nm-thick rubrene layer. Figure 3d shows the conductance versus bias curves for a device with a 20 nm-thick rubrene layer measured at 300 (black curve) and 150 K (red curve). A primary difference was the downshift of the curve at 150 K because of the increase of the resistance. Our observation was similar to the results reported previously using a 15 nm-thick rubrene layer.[28]

To investigate the spin-dependent electron transfer behaviors, a series of rubrene-based devices with different rubrene-layer thicknesses (2, 5, 10, and 20 nm) was fabricated, and the MR effects of these devices were measured at 300, 250, 200, and 150 K, as depicted in Figure 4. The MR ratio decreased monotonously with increasing rubrene-layer thickness, as shown in Figure 4a. The largest MR ratio was approximately 6% for a rubrene-layer-thickness of 2 nm at room temperature, and the MR ratio decreased to 0.6% for devices with a 20 nm-thick rubrene layer. The MR ratio dependence on the measurement temperature is plotted in Figure 4b. The MR ratio for devices with 2 and 6 nm thick rubrene layers exhibited a sharper increase with decreasing measurement temperature in comparison with those of devices with thicker rubrene layers of 12 and 20 nm. The devices with rubrene layer thickness below 2 nm usually failed. This may be due to a discontinuous film of thinner rubrene layer or a thin "ill-defined layer"[13] for rubrene/Co interface. In the following two paragraphs, we will try to discuss the possible spin transport mechanism in these OSVs.

Several theoretical methods have been proposed to analyze the related factors affecting on the spin-dependent transport mechanisms, tunneling or diffusion, in disordered OSs.[43−47] It has been demonstrated that the site-energy disorder or positional disorder, spin mixing, and the exchange coupling between localized polarons contribute to the spin-dependent transport. These theories have promoted an understanding of the spin transport behavior in organic spintronics. In contrast, there is still no generally accepted experimental method to clearly clarify the spin-dependent transport mechanism in OSVs. Therefore, it is very difficult to illustrate the exact spin electron transport mechanism in the present rubrene-based devices. Here, we speculate on the possible spin transport mechanism. In general, the thickness of the spacer layer in spin valves, around several nanometers, is in the tunneling transport range. With increasing spacer-layer thickness, the transport behaviors become complicated, and the tunneling mechanism changes from single-step tunneling to multiple-step tunneling. For spacer-layer thickness over several tens of nanometers, diffusion mechanisms play a dominant role. In this regard,

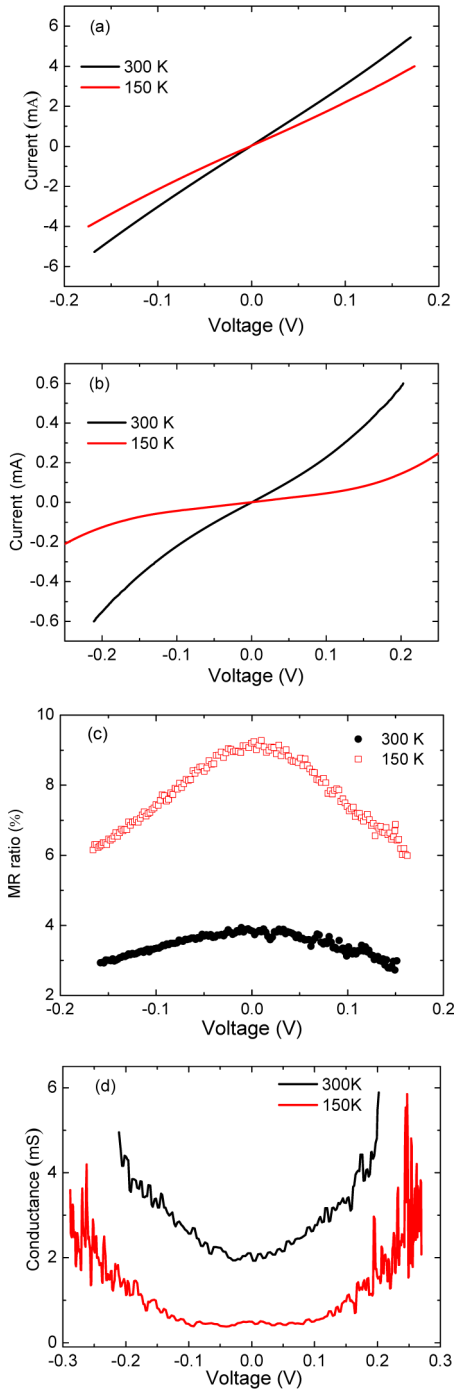

Figure 3. Nonlinear current−voltage curves for spin valves with (a) 6 nm-thick and (b) 20 nm-thick rubrene layers, which were measured at 300 and 150 K, respectively. (c) Bias-voltage dependence of MR ratios at 300 K (black circles) and 150 K (red squares) for a device with of a 6 nm-thick rubrene layer. (d) Conductance versus bias curves for a device with a 20 nm-thick rubrene layer measured at 300 (black curve) and 150 K (red curve).

Schoonus and coauthors have reported a decrease in the MR ratio with increasing Alq_3 layer thicknesses ranging from 1 to 4 nm.[38] They hypothesized that this decrease was caused by a transition in the spin-dependent transport from single-step tunneling to multiple-step tunneling with increasing Alq_3 layer thickness. This explanation agrees well with the reports in Alq_3 based spin valves from Moodera's group[33] and Coey's group.[39]

DOI: 10.1021/am508173j
ACS Appl. Mater. Interfaces 2015, 7, 4685−4692

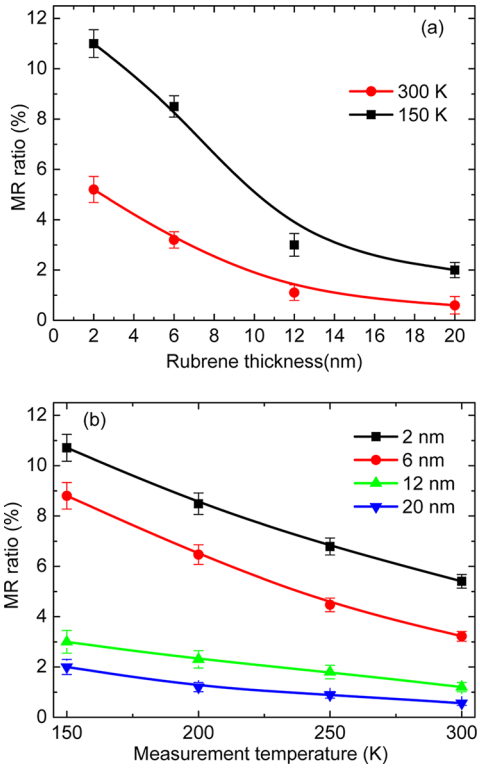

Figure 4. (a) Dependence of the magnetoresistance ratios on the rubrene-layer thickness measured at 300 (red circles) and 150 K (black squares). (b) Measurement temperature dependence of the magnetoresistance ratios for devices with different rubrene-layer thicknesses. The lines serve as a visual guide.

In C_{60}-based spin valve, multiple-step tunneling mechanism occurs when the organic layer thickness is over ~4 nm.[40,43] In the present rubrene-based devices, single-step tunneling is most probably dominant in the devices with a 2 nm-thick rubrene layer. Upon increasing the rubrene thickness, the multiple-step tunneling processes become stronger, thereby resulting in a decrease in the MR ratios. The XRD measurements indicates the rubrene layers in this report were of amorphous structure, agreeing with our previous result.[48]

The defects appear in the amorphous rubrene-layer, which will also affect the spin-dependent transport behaviors.[22,26,28,47] This effect could occurs in our OSVs and may be stronger with increasing rubrene layer thickness. The observed temperature dependence of the MR ratios for the spin valves with 2 and 6 nm thick rubrene layers differs from those for spin valves with the 12 and 20 nm thick rubrene layers, as shown in Figure 4b. This is probably due to change in the spin-dependent transport mechanism based on the competition of above factors.

For inorganic spin valves, the MR ratio can usually be increased by postannealing. The resulting increase is mainly due to decrease in spin scattering by increasing the interface quality after annealing. Consequently, we annealed the rubrene-based spin valves in vacuum for 6 min at 363 K to enhance the MR ratios. After the sample device was cooled to room temperature, its MR curve was measured again. Figure 5a shows the results measured at 300 K for the device with a 6 nm-thick rubrene layer before and after annealing. We note that the shape of the MR curve after annealing is same as that before annealing. However, it is also noteworthy that the MR ratio reduces from 3.3% to 1.9% after annealing. We also measured

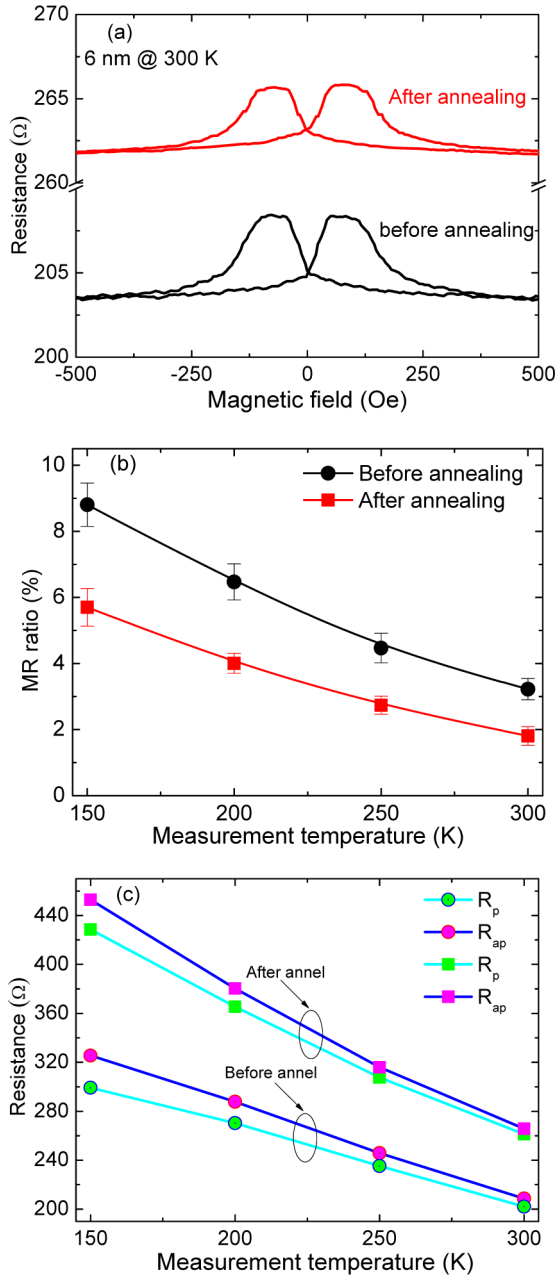

Figure 5. (a) Magnetoresistance curves measured at 300 K for spin valves with a 6 nm-thick rubrene layer before annealing (black lines) and after annealing (red lines). Measurement temperature dependence of (b) magnetoresistance ratios and (c) resistances for the device before and after annealing. Resistances for parallel and antiparallel states are denoted as R_p and R_{ap}, respectively. The lines serve as a visual guide.

the MR curves at low temperatures, and their MR ratios are plotted in Figure 5b. We find that the MR ratios decrease after annealing. Further, it is noted that the device resistances for both parallel and antiparallel states increase after annealing compared to the corresponding values before annealing, as summarized in Figure 5c. This indicates that the spin scattering becomes stronger after annealing compared with that before annealing. The rubrene layers annealed with the same condition were still of amorphous structure checked by the XRD measurement (see Supporting Information Figure S2), which is owing to the low annealing temperature. It should also be

DOI: 10.1021/am508173j
ACS Appl. Mater. Interfaces 2015, 7, 4685−4692

noted that this temperature is hard to change the interface quality for Fe_3O_4/Al−O layers because the bilayer film were directly annealed at 623 K after deposition.

To further explore the possible reasons for the increase in spin scattering, atomic force microscopy was utilized to inspect the rubrene films. Figures 6a and 6b show the morphology of

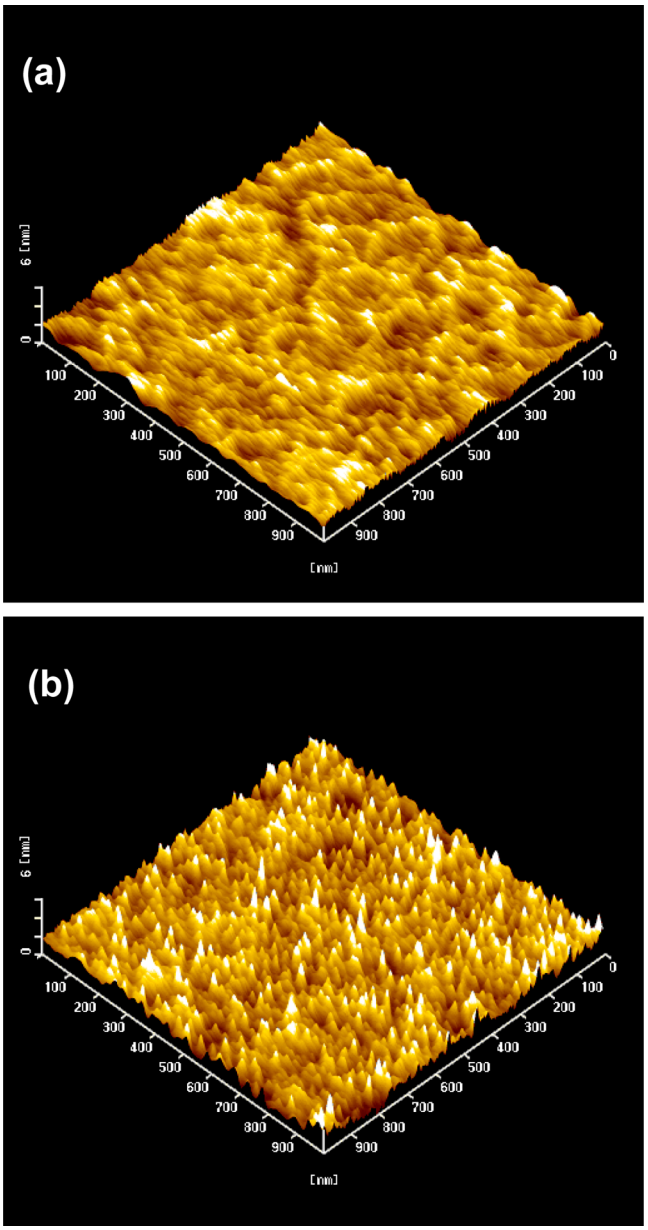

Figure 6. Atomic force microscopy images of rubrene layer (100 nm) deposited on MgO/Fe_3O_4/Al−O (a) before and (b) after annealing.

the rubrene films before and after annealing. We note that the surface of the film is very flat and uniformly smooth before annealing. But it becomes very rough after annealing. We observed that the roughness of the film increased from 0.25 to 0.41 nm, and the maximum height between peak and valley increased from 3 to 5 nm after annealing. Consequently, we deduced that the increased roughness after annealing increases the electron scattering at the interface, which probably leads to the observed decrease in the MR ratios. The increase of spin scattering reduces the electron number through the devices, agreeing with the increase of device resistances, as shown in Figure 5c. It should be noted that the increased roughness is mainly attributed to the inhomogeneous growth of rubrene in the film during annealing. A theoretical calculation made by Yu predicted that the spin diffusion length could be over 430 nm in rubrene film.[49] For actual rubrene devices, small spin transport (diffusion and tunneling) lengths were generally observed.[20−28] In this report, MR response disappears for the device with rubrene layer thickness over 20 nm, agreeing with the these experimental results. The device performance is related to the microstructure of film, such as molecular arrangement[17] and the impurity band in the organic layer.[22,26,28,47] In this regard, the fabrication technique should be further explored to obtain high-quality films for OSVs. If a rubrene film with single-crystal structure was fabricated and used for spin devices, the spin transport length and MR response could be significantly enhanced.

CONCLUSIONS

We fabricated a vertical spin-valve device with a Fe_3O_4/Al−O/rubrene/Co stacking structure, and achieved a large MR ratio of approximately 6% at room temperature. The dependence of the MR ratios on the rubrene-layer thickness was studied. It was found that the MR ratios monotonously decrease with increasing rubrene-layer thickness. The decrease of MR ratio is mainly due to the change of the spin-dependent transport mechanism from single-step tunneling to multiple-step tunneling with increasing rubrene-layer thickness. In addition, we noticed the MR ratios in the OSVs after annealing were smaller than those of their counterparts before annealing. This is most probably due to the increase of interface spin scattering induced by large surface roughness after annealing. Our results will deepen the understanding of spin-dependent electron transport in organic spin devices

ASSOCIATED CONTENT

Supporting Information

Nonlinear current−voltage curves and XRD measurements. This material is available free of charge via the Internet at http://pubs.acs.org.

AUTHOR INFORMATION

Corresponding Authors

*E-mail: zhangxm@atm.neu.edu.cn
*E-mail: qingw@smm.neu.edu.cn.

Notes

The authors declare no competing financial interest.

ACKNOWLEDGMENTS

This work was partially supported by a research grant from the Murata Science Foundation, WPI-AIMR Fusion Research Grant, the National Natural Science Foundation of China (No. 51471046), the Startup Foundation for Talents from Northeastern University of China, and the Changjiang Scholars and Innovative Research Team in University (No. IRT0713).

REFERENCES

(1) Dediu, V.; Murgia, M.; Matacotta, F. C.; Taliani, C.; Barbanera, S. Room Temperature Spin Polarized Injection in Organic Semiconductors. *Solid State Commun.* **2002**, *122*, 181−184.

(2) Xiong, Z. H.; Wu, D.; Vardeny, Z. V.; Shi, J. Giant Magnetoresistance in Organic Spin-Valves. *Nature* **2004**, *427*, 821−824.

DOI: 10.1021/am508173j
ACS Appl. Mater. Interfaces 2015, 7, 4685−4692

(3) Barraud, C.; Seneor, P.; Mattana, R.; Fusil, S.; Bouzehouane, K.; Deranlot, C.; Graziosi, P.; Hueso, L.; Bergenti, I.; Dediu, V.; Petroff, F.; Fert, A. Unravelling the Role of The Interface for Spin Injection into Organic Semiconductors. *Nat. Phys.* **2010**, *6*, 615−620.
(4) Steil, S.; Großmann, N.; Laux, M.; Ruffing, A.; Steil, D.; Wiesenmayer, M.; Mathias, S.; Monti, O. L. A.; Cinchetti, M.; Aeschlimann, M. Spin-Dependent Trapping of Electrons at Spinterfaces. *Nat. Phys.* **2013**, *9*, 242−247.
(5) Raman, K. V.; Kamerbeek, A. M.; Mukherjee, A.; Atodiresei, N.; Sen, T. K.; Lazic, P.; Caciuc, V.; Michel, R.; Stalke, D.; Mandal, S. K.; Blugel, S.; Munzenberg, M.; J. Moodera, S. Interface-Engineered Templates for Molecular Spin Memory Devices. *Nature* **2013**, *493*, 509−513.
(6) Li, F.; Li, T.; Guo, X. Y. Vertical Graphene Spin Valves Based on $La_{2/3}Sr_{1/3}MnO_3$ Electrodes. *ACS Appl. Mater. Interfaces* **2014**, *6*, 1187−1192.
(7) Singh, A. K.; Eom, J. Negative Magnetoresistance in a Vertical Single-Layer Graphene Spin Valve at Room Temperature. *ACS Appl. Mater. Interfaces* **2014**, *6*, 2493−2496.
(8) Li, F. Effect of Substrate Temperature on the Spin Transport Properties in C_{60}-Based Spin Valves. *ACS Appl. Mater. Interfaces* **2013**, *5*, 8099−8104.
(9) Sun, D. L.; Ehrenfreund, E.; Vardeny, Z. V. The First Decade of Organic Spintronics Research. *Chem. Commun.* **2014**, *50*, 1781−1793.
(10) Shi, S.; Sun, Z.; Bedoya-Pinto, A.; Graziosi, P.; Li, X.; Liu, X.; Fahlman, M. Hybrid Interface States and Spin Polarization at Ferromagnetic Metal−Organic Heterojunctions: Interface Engineering for Efficient Spin Injection in Organic Spintronics. *Adv. Funct. Mater.* **2014**, *24*, 4812−4821.
(11) Nguyen, T. D.; Hukic-Markosian, G.; Wang, F. J.; Wojcik, L.; Li, X.-G.; Ehrenfreund, E.; Vardeny, Z. V. Isotope Effect in Spin Response of π-conjugated Polymer Films and Devices. *Nat. Mater.* **2010**, *9*, 345−352.
(12) Zhang, X. M.; Mizukami, S.; Ma, Q. L.; Kubota, T.; Oogane, M.; Naganuma, H.; Ando, Y.; Miyazaki, T. Spin-Dependent Transport Behavior in C_{60} and Alq_3 Based Spin Valves with a Magnetite Electrode. *J. Appl. Phys.* **2014**, *115*, No. 172608.
(13) Dediu, V.; Hueso, L. E.; Bergenti, I.; Riminucci, A.; Borgatti, F.; Graziosi, P.; Newby, C.; Casoli, F.; De Jong, M. P.; Taliani, C.; Zhan, Y. Room-Temperature Spintronic Effects in Alq_3-Based Hybrid Devices. *Phys. Rev. B* **2008**, *78*, No. 115203.
(14) Dediu, V.; Hueso, L. E.; Bergenti, I.; Taliani, C. Spin Routes in Organic Semiconductors. *Nat. Mater.* **2009**, *8*, 707−716.
(15) Zhang, X. M.; Mizukami, S.; Kubota, T.; Ma, Q. L.; Oogane, M.; Naganuma, H.; Ando, Y.; Miyazaki, T. Observation of a Large Spin-Dependent Transport Length in Organic Spin Valves at Room Temperature. *Nat. Commun.* **2013**, *4*, 1392.
(16) Liu, Y. H.; Watson, S. M.; Lee, T.; Gorham, J. M.; Katz, H. E.; Borchers, J. A.; Fairbrother, H. D.; Reich, D. H. Correlation Between Microstructure and Magnetotransport in Organic Semiconductor Spin-Valve Structures. *Phys. Rev. B* **2009**, *79*, No. 075312.
(17) Vehoff, T.; Baumeier, B.; Troisi, A.; Andrienko, D. Charge Transport in Organic Crystals: Role of Disorder and Topological Connectivity. *J. Am. Chem. Soc.* **2010**, *132*, 11702−11708.
(18) Zheng, Y. H.; Wudl, F. Organic Spin Transporting Materials: Present and Future. *J. Mater. Chem. A* **2014**, *2*, 48−57.
(19) Yu, Z. G. Spin-Orbit Coupling, Spin Relaxation, and Spin Diffusion in Organic Solids. *Phys. Rev. Lett.* **2011**, *106*, No. 106602.
(20) Yoo, J.-W.; Chen, C.-Y.; Jang, H. W.; Bark, C. W.; Prigodin, V. N.; Eom, C. B.; Epstein, A. J. Spin Injection/Detection Using an Organic-based Magnetic Semiconductor. *Nat. Mater.* **2010**, *9*, 638−642.
(21) Yoo, J.-W.; Jang, H. W.; Prigodin, V. N.; Kao, C.; Eom, C. B.; Epstein, A. J. Tunneling vs. Giant Magnetoresistance in Organic Spin Valve. *Synth. Met.* **2010**, *160*, 216−222.
(22) Yoo, J.-W.; Jang, H. W.; Prigodin, V. N.; Kao, C.; Eom, C. B.; Epstein, A. J. Giant Magnetoresistance in Ferromagnet/Organic Semiconductor/Ferromagnet Heterojunctions. *Phys. Rev. B* **2009**, *80*, No. 205207.
(23) Li, B.; Kao, C. Y.; Lu, Y.; Yoo, J.-W.; Prigodin, V. N.; Epstein, A. J. Room-Temperature Organic-Based Spin Polarizer. *Appl. Phys. Lett.* **2011**, *99*, No. 153503.
(24) Li, B.; Kao, C. Y.; Yoo, J.-W.; Prigodin, V. N.; Epstein, A. J. Magnetoresistance in an All-Organic-Based Spin Valve. *Adv. Mater.* **2011**, *23*, 3382−3386.
(25) Raman, K. V.; Chang, J.; Moodera, J. S. New Method of Spin Injection into Organic Semiconductors using Spin Filtering Tunnel Barriers. *Org. Electron.* **2011**, *12*, 1275−1278.
(26) Alam, K. M.; Bodepudi, S. C.; Starko-Bowes, R.; Pramanik, S. Suppression of Spin Relaxation in Rubrene Nanowire Spin Valves. *Appl. Phys. Lett.* **2012**, *101*, No. 192403.
(27) Shim, J. H.; Raman, K. V.; Park, Y. J.; Santos, T. S.; Miao, G. X.; Satpati, B.; Moodera, J. S. Large Spin Diffusion Length in an Amorphous Organic Semiconductor. *Phys. Rev. Lett.* **2008**, *100*, No. 226603.
(28) Lin, R.; Wang, F.; Rybicki, J.; Wohlgenannt, M.; Hutchinson, K. A. Distinguishing Between Tunneling and Injection Regimes of Ferromagnet/Organic Semiconductor/Ferromagnet Junctions. *Phys. Rev. B* **2010**, *81*, No. 195214.
(29) Yanase, A.; Siratori, K. Band Structure in the High Temperature Phase of Fe_3O_4. *J. Phys. Soc. Jpn.* **1984**, *53*, 312−317.
(30) Zhang, Z.; Satpathy, S. Electron States, Magnetism, and the Verwey Transition in Magnetite. *Phys. Rev. B* **1991**, *44*, 13319−13331.
(31) Seneor, P.; Fert, A.; Maurice, J.-L.; Montaigne, F.; Petroff, F.; Vaurès, A. Large Magnetoresistance in Tunnel Junctions with an Iron Oxide Electrode. *Appl. Phys. Lett.* **1999**, *74*, No. 4017.
(32) Dedkov, Yu. S.; Rüdiger, U.; Güntherodt, G. Evidence for the Half-Metallic Ferromagnetic State of Fe_3O_4 by Spin-Resolved Photoelectron Spectroscopy. *Phys. Rev. B* **2002**, *65*, No. 064417.
(33) Santos, T. S.; Lee, J. S.; Migdal, P.; Lekshmi, I. C.; Satpati, B.; Moodera, J. S. Room-Temperature Tunnel Magnetoresistance and Spin-Polarized Tunneling through an Organic Semiconductor Barrier. *Phys. Rev. Lett.* **2007**, *98*, No. 016601.
(34) Hong, J.-Y.; Chang, Y.-M.; Chuang, C.-H.; Li, K.-S.; Jhang, Y.-C.; Shiu, H.-W.; Chen, C.-H.; Chiang, W.-C.; Lin, M.-T. Depth Profiling Photoelectron-Spectroscopic Study of an Organic Spin Valve with a Plasma-Modified Pentacene Spacer. *J. Phys. Chem. C* **2012**, *116*, 21157−21161.
(35) Wang, T. X.; Wei, H. X.; Zeng, Z. M.; Han, X. F.; Hong, Z. M.; Shi, G. Q. Magnetic/Nonmagnetic/magnetic Tunnel Junction Based on Hybrid Organic Langmuir-Blodgett-Films. *Appl. Phys. Lett.* **2006**, *88*, No. 242505.
(36) Yue, F. J.; Shi, Y. J.; Chen, B. B.; Ding, H. F.; Zhang, F. M.; Wu, D. Manipulating Spin Injection into Organic Materials through Interface Engineering. *Appl. Phys. Lett.* **2012**, *101*, No. 022416.
(37) Majumdar, S.; Laiho, R.; Laukkanen, P.; Väyrynen, I. J.; Majumdar, H. S.; Österbacka, R. Application of Regioregular Polythiophene in Spintronic Devices: Effect of Interface. *Appl. Phys. Lett.* **2006**, *89*, No. 122114.
(38) Schoonus, J. J. H. M.; Lumens, P. G. E.; Wagemans, W.; Kohlhepp, J. T.; Bobbert, P. A.; Swagten, H. J. M.; Koopmans, B. Magnetoresistance in Hybrid Organic Spin Valves at the Onset of Multiple-Step Tunneling. *Phys. Rev. Lett.* **2009**, *103*, 146601.
(39) Szulczewski, G.; Tokuc, H.; Oguz, K.; Coey, J. M. D. Magnetoresistance in Magnetic Tunnel Junctions with an Organic Barrier and a MgO Spin Filter. *Appl. Phys. Lett.* **2009**, *95*, No. 202506.
(40) Gobbi, M.; Golmar, F.; Llopis, R.; Casanova, F.; Hueso, L. E. Room-Temperature Spin Transport in C_{60}-Based Spin Valves. *Adv. Mater.* **2011**, *23*, 1609−1613.
(41) Miyazaki, T.; Tezuka, N. Giant Magnetic Tunneling Effect in $Fe/Al_2O_3/Fe$ junction. *J. Magn. Magn. Mater.* **1995**, *139*, L231−L234.
(42) Tsunoda, M.; Nishikawa, K.; Ogata, S.; Takahashi, M. 60% Magnetoresistance at Room Temperature in Co−Fe/Al−O/Co−Fe Tunnel Junctions Oxidized with Kr−O_2 Plasma. *Appl. Phys. Lett.* **2002**, *80*, 3135.
(43) Lan Anh Tran, T.; Quyen Le, T.; Sanderink, J. G. M.; van der Wiel, W. G.; De Jong, M. P. The Multistep Tunneling Analogue of

DOI: 10.1021/am508173j
ACS Appl. Mater. Interfaces 2015, 7, 4685−4692

Conductivity Mismatching Organic Spin Valves. *Adv. Funct. Mater.* **2012**, *22*, 1180−1189.
(44) Bobbert, P. A.; Wagemans, W.; Van Oost, F. W. A.; Koopmans, B.; Wohlgenannt, M. Theory for Spin Diffusion in Disordered Organic Semiconductors. *Phys. Rev. Lett.* **2009**, *102*, No. 156604.
(45) Harmon, N. J.; Flatté, M. E. Spin-Flip Induced Magnetoresistance in Positionally Disordered Organic Solids. *Phys. Rev. Lett.* **2012**, *108*, No. 186602.
(46) Harmon, N. J.; Flatté, M. E. Distinguishing Spin Relaxation Mechanisms in Organic Semiconductors. *Phys. Rev. Lett.* **2013**, *110*, No. 176602.
(47) Yu, Z. G. Impurity-Band Transport in Organic Spin Valves. *Nat. Commun.* **2014**, *5*, 4842.
(48) Zhang, X. M.; Mizukami, S.; Kubota, T.; Ma, Q. L.; Naganuma, H.; Oogane, M.; Ando, Y.; Miyazaki, T. Large Change of Perpendicular Magnetic Anisotropy in Cobalt Ultrathin Film Induced by Varying Capping Layers. *J. Appl. Phys.* **2012**, *111*, No. 07B320.
(49) Yu, Z. G. Spin-Orbit Coupling and Its Effects in Organic Solids. *Phys. Rev. B* **2012**, *85*, No. 115201.

DOI: 10.1021/am508173j
ACS Appl. Mater. Interfaces 2015, 7, 4685−4692